



Influences of El Niño–Southern Oscillation on summertime ozone pollution over central-eastern China during 1950–2014

Yuxuanzi Wang¹ · Yingying Yan¹ · Jintai Lin² · Shaofei Kong^{1,3} · Aili Song¹ · Jing Ma¹

Received: 23 May 2022 / Accepted: 10 August 2022

© The Author(s), under exclusive licence to Springer-Verlag GmbH Germany, part of Springer Nature 2022

Abstract

Summertime ozone pollution has become increasingly severe over many parts of China in recent years. Due to lack of historical ozone observations, few studies have analyzed the linkage between natural climate variability and ozone levels for a long time series. This study uses the simulation datasets from CMIP6 to explore the effects of El Niño–Southern Oscillation (ENSO) on summertime (June/July/August) surface ozone concentrations in central-eastern China (CEC; 20°N–42°N, 100°E–123°E) during the period of 1950–2014. Our results show that, after excluding the emission-related trend, the detrended summertime daily mean surface ozone concentrations averaged over CEC in El Niño years (30.69 ppb) are higher than those in La Niña events (29.34 ppb). Compared to the summertime mean ozone of 1950–2014 (30.25 ppb), the maximum anomalies in CMIP6 are 2.88 ppb (9.52% higher) and –5.52 ppb (18.25% lower) in El Niño and La Niña years, respectively. In addition, the summertime MDA8 ozone of CEC is significantly correlated with the central-eastern equatorial Pacific SST (5°N–5°S, 170°W–120°W) ($R=0.29$, P -value = 0.02). Such ozone increases/declines in El Niño/La Niña years are also found in satellite observations of OMI ozone. The results show that the ENSO affects the large-scale circulations over central-eastern China, which regulate the regional atmospheric stability and meteorological conditions (including horizontal wind fields, geopotential height, vertical velocity, surface air temperature, and precipitation) to influence the efficiency of ozone photochemical formation and transport. Our study makes better estimation and attribution of future surface ozone pollution in China.

Keywords Historical ozone · CMIP6 · El Niño · La Niña · Summertime surface ozone pollution · Central-eastern China

Introduction

Ozone acts as both a greenhouse gas and an ambient ground-level pollutant (Lippmann 1989) harming human health, agriculture, and ecosystems (Liu et al. 2018; Nuvolone et al. 2018; Emberson 2020). Surface ozone concentrations are

controlled by the complex combination of chemistry, deposition, and transport (Davies et al. 1992; Yan et al. 2016). Ozone is produced via the reaction of volatile organic compounds (VOCs) and nitrogen oxides ($\text{NO}_x = \text{NO} + \text{NO}_2$), which are the main reactants in the ozone photochemical oxidation (Sillman et al. 1990; Shen et al. 2019). Moreover, ozone has an important impact on the atmospheric oxidation, which can influence the lifetime of trace gases and further regulate the atmospheric environment and climate change, as the hydroxyl radical (OH) participates in ozone formation and ozone is also a precursor for the OH (Wennberg and Dabdub 2008; Wang et al. 2017). In addition, surface ozone has become one of the most serious air pollution worldwide in the past few decades (Li et al. 2019; Lin et al. 2017; Yan et al. 2018, 2019), and attracted more and more attention from society and scientific community (Ma et al. 2012, 2016; Monks et al. 2015; Sun et al. 2019; Yan et al. 2021).

It is widely recognized that surface ozone concentrations are closely related to the meteorological conditions. Many

Responsible Editor: Gerhard Lammel

✉ Yingying Yan
yanyingying@cug.edu.cn

¹ Department of Atmospheric Science, School of Environmental Sciences, China University of Geosciences, Wuhan 430074, China

² Laboratory for Climate and Ocean-Atmosphere Studies, Department of Atmospheric and Oceanic Sciences, School of Physics, Peking University, Beijing 100871, China

³ Department of Environmental Science and Engineering, School of Environmental Studies, China University of Geosciences, Wuhan 430074, China

researches have extensively studied the effects of meteorological factors on the photochemical production and transport of ozone (David and Nair 2011; Otero et al 2016; Li et al. 2017; Lu et al. 2019). On a local scale, ozone concentrations are higher when the sunlight is strong, the humidity is relatively low, and the temperature is high, which are favorable to ozone formation (Duan et al. 2008; Jacob and Winner 2009; He et al. 2017; Li et al. 2017). Meanwhile, the wind speed and direction also play a significant role in the accumulation and removal of pollutants on a regional scale (Wang et al. 2010; Ma et al. 2011; Li et al. 2017). Thus the meso-scale and large-scale atmospheric circulation can decide the distribution and variation of ozone as well as ozone precursors (Zhang et al. 2012; Shu et al. 2016; Liao et al. 2017; Li et al. 2020; Han et al. 2020; Wang et al. 2021). For instance, for the Pearl River Delta (PRD), the tropical cyclones can bring more pollutants from inland through the anti-clockwise circulation, and also provide favorable meteorological conditions for ozone photochemical formation on the edge of typhoon (Ding et al. 2004). Natural climate variability affects the meteorological conditions and thus surface ozone concentrations. For example, the East Asian Monsoon (EAM) regulates the seasonal lower tropospheric ozone over coastal South China by impacting the transport of pollutants (Zhou et al. 2013). And the East Asian Summer Monsoon (EASM) associated with the precipitation and wind fields accounts of 81.5% for the reduction of summertime surface ozone in southern China (Chen et al. 2020). The GEOS-Chem chemical transport model has also indicated that the intensity of EASM has a significant positive correlation with summertime ozone during 1986–2006 in China (Yang et al. 2014). While over the Asia–Pacific region, the summer monsoons influence the position of pollutants transition zone caused by the combination of zonal winds, rain belt, and anthropogenic emissions (Hou et al. 2015). Therefore, in order to better estimate the future trend of ozone pollution in China, it is significant to investigate the influence of climate system variability on historical surface ozone concentrations.

El Niño and La Niña are two phases of the tropical sea surface temperature (SST) variability on the interannual timescale (Philander 1985). During El Niño, the central-eastern equatorial Pacific SST is warmer than its climatological level, while cooler in La Niña (Philander 1985). The interannual variability of SST can affect the Hadley Cell (Quan et al. 2004), which will cause changes in regional temperature and precipitation, and further influence the global climate (Bjerknes 1972; Chandra et al. 1998; Chang et al. 2000; Sudo and Takahashi 2001; Zhai et al. 2016). Many studies have discussed the relationships between ozone and interannual variability of tropical SST (Zeng and Pyle 2005; Koumoutsaris et al. 2008; Hitchman and Rogal 2010; Lee et al. 2010; Voulgarakis et al. 2010; Ziemke et al. 2010; Oman et al. 2011; Voulgarakis

et al. 2011; Xie et al. 2014; Zhang et al. 2015; Ziemke et al. 2015; Shen and Mickley 2017; Xu et al. 2017). Ziemke et al. (2010) used the tropospheric column ozone (TCO) retrieved from satellite remote sensing to derive a new ENSO index called Ozone ENSO Index (OEI), which is the difference in TCO between the western Pacific-Indian Ocean region (15°S–15°N, 70°E–140°E) and the central-eastern Pacific region (15°S–15°N, 110°W–180°W). Oman et al. (2011) also discussed the relationship between tropical tropospheric ozone and ENSO based on the Global Modeling Initiative (GMI) simulations, and obtained the OEI. The OEI results from both measurements and simulations are very similar to the Niño 3.4 Index calculated by National Oceanic and Atmospheric Administration (NOAA), with correlations of 0.84 and 0.86, respectively (Oman et al. 2011). In addition, the northern mid-latitude ozone can be impacted by ENSO in JFM (January, February, and March) (Zhang et al. 2015). Zhang et al. (2015) showed that during the El Niño, the TCO are higher in southern United States, northeastern Africa, North Pacific, and East Asia than their climatological values, but lower over the central Europe and North Atlantic. On the contrary, during La Niña events, there are opposite results. These studies have focused on the tropospheric ozone, and only a few recent studies have examined the effects of ENSO on surface ozone (Jiang and Li 2022; Li et al. 2022; Yang et al. 2022), especially on the long time series of summertime surface ozone, due to lack of historical ozone observations.

In this study, we explore the effects of the ENSO (defined by anomalies of central-eastern equatorial Pacific SST) on summertime (June/July/August) surface ozone in central-eastern China (CEC; 20°N–42°N, 100°E–123°E) during the period 1950–2014. Firstly, we use the modeled historical SST from CMIP6 (Coupled Model Intercomparison Project Phase 6) to calculate the Niño Index over the central-eastern equatorial Pacific (Niño 3.4 region: 5°N–5°S, 170°W–120°W). After defining El Niño and La Niña events through the CMIP6 Niño Index (CNI), we discuss the distribution and variation of modeled historical summertime surface ozone concentrations over CEC in El Niño and La Niña years, respectively. To evaluate the simulated results, we also use surface ozone retrieved from satellite to do the same analysis. Finally, the meteorological conditions from CMIP6 are analyzed to understand the causes of ozone differences during El Niño and La Niña.

Data and methods

Data

We download the modeled historical (1950–2014) data from CMIP6 (<https://cera-www.dkrz.de/WDCC/ui/cerasearch/cmip6?input=CMIP6.CMIP.MOHC.UKESM1-0-LL.histo>

tical/), including hourly surface ozone and monthly mean sea surface temperature, horizontal wind fields, geopotential height, vertical velocity, surface air temperature, and precipitation. The horizontal resolution of the CMIP6 data is 1.25° longitude \times 1.25° latitude. As there are only four models (UKESM1-0-LL, 1850–2014; MPI-ESM-1-2-HAM, 1850–2014; GFDL-ESM4, 1980–2014; and EC-Earth3-AerChem, 1850–2014) provided historical surface ozone in the CMIP6 website (<https://esgf-node.llnl.gov/projects/cmip6/>), we use the MPI-ESM-1-2-HAM and EC-Earth3-AerChem data to do the same analysis to verify the reliability of the simulated data we used (UKESM1-0-LL).

Many previous studies have used the CMIP6 (the newest revision of CMIP) simulated data to investigate the global climate of the past, current, and future (Eyring et al. 2016; O'Neill et al. 2016; Bracegirdle et al. 2020; Butchart et al. 2020; Narsey et al. 2020). In order to make a comparison between simulations and measurements, we use the surface ozone satellite retrieval data from the space-based Ozone Monitoring Instrument (OMI) during the period of 2005–2017 (<https://www.cfa.harvard.edu/atmosphere/>). The grid resolution of OMI data is 0.25° longitude \times 0.25° latitude. Besides, we also use the NOAA Niño 3.4 index (https://origin.cpc.ncep.noaa.gov/products/analysis_monitoring/ensostuff/ONI_v5.php/) to identify the actually occurred El Niño and La Niña events. In order to verify whether the ENSO signal and related changes in meteorological parameters of CMIP6 are consistent with observations, we also use the monthly averaged data (0.25° longitude \times 0.25° latitude) from 2005 to 2017 generated by European Centre for Medium-Range Weather Forecasts (ERA5; <https://www.ecmwf.int/en/forecasts/datasets/reanalysis-datasets/era5/>) to conduct the same analysis as CMIP6, including horizontal wind fields (925 hPa), geopotential height (925 hPa), vertical velocity (925 hPa), surface air temperature (1000 hPa), and specific humidity (1000 hPa). In this study, the ozone indices we used is daily mean ozone, unless otherwise specified in the text.

A comparison of the summertime ozone concentrations between OMI and CMIP6 over 2005–2014 shows a good correlation ($R=0.47$ and P -value < 0.05) over China (Fig. 1), although with model overestimation (underestimation) in Western (Northern) China. Griffiths et al. (2021) have also compared the CMIP6 model ensemble to five in-situ stations that have long-term surface ozone observations, including Mauna Loa, Hawaii, USA (1957–present); the South Pole (1961–present); Barrow, Alaska, USA (1973–present); Cape Matatula, Tutuila, American Samoa (1975–present); and Cape Grim, Tasmania, Australia (1982–present). Their results show temporal correlation coefficients between 0.29 (American Samoa, with the mean normalized bias error of 41.4%) and 0.74 (Hawaii, with the mean normalized bias error of 7.9%), and that the historical simulations capture

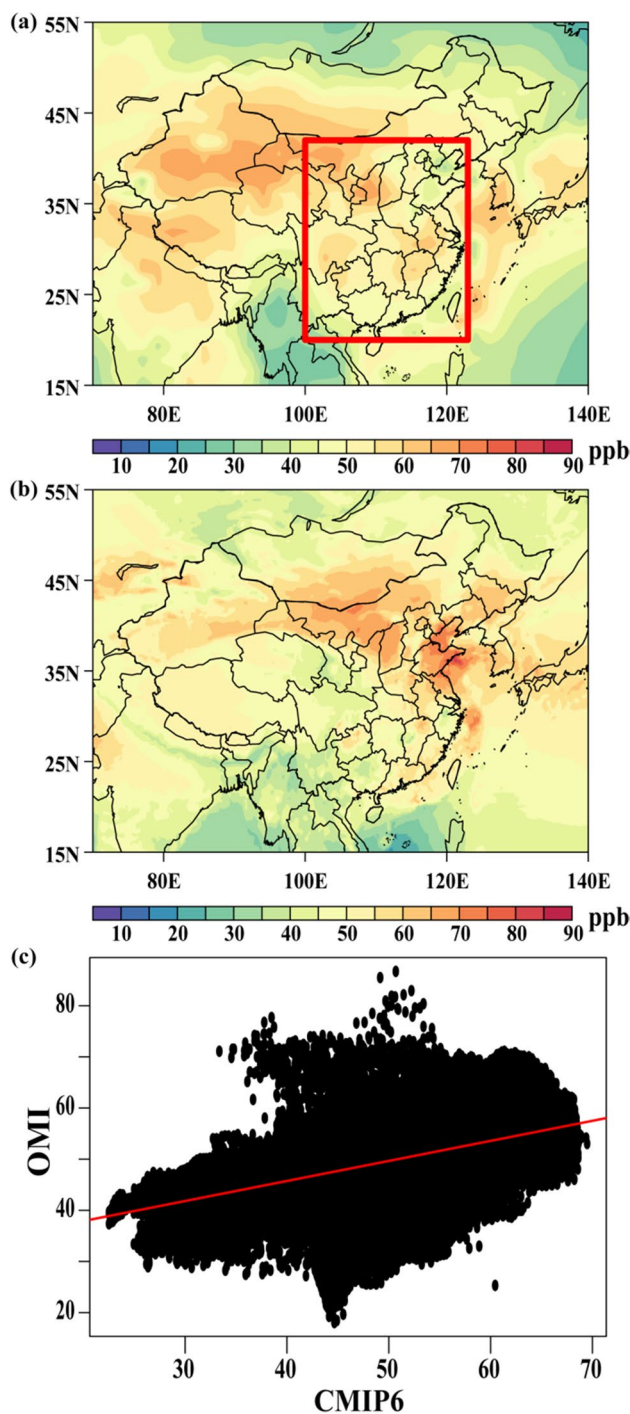


Fig. 1 Spatial distribution of summertime mean surface ozone averaged over 2005–2014 based on CMIP6 simulations (a) and OMI observations (b). (c) The correlation between OMI and CMIP6 over the whole domain from 2005 to 2014 ($R=0.47$, P -value < 0.05). The red frame marks the area of central-eastern China (20°N – 42°N , 100°E – 123°E)

the observed interdecadal trends attributed to emissions and climate variability. Our previous study showed strong correlation between OMI and ground observations from the

China's Ministry of Ecology and Environment ($R=0.81$, P -value < 0.05) over the period of 2016–2017. Moreover, the trend of surface ozone from CMIP6 is consistent with the measurements from 2005 to 2019 in China (Wang et al. 2021).

In addition, the increasing trend of surface ozone during 1950–2014 is mainly related to emission, and only a slight trend contributed by meteorology (Wang et al. 2021). Therefore, in the following text, in order to exclude the impact of anthropogenic emission, we remove the long-term trend of ozone before the discussion of meteorological influences on ozone (see details in supplementary Section 1). The trends of summertime surface ozone during the period of 1950–2014 are 0.25 ppb yr^{-1} , 0.46 ppb yr^{-1} , and 0.36 ppb yr^{-1} over the north (31°N – 42°N , 100°E – 123°E), south (20°N – 31°N , 100°E – 123°E), and whole central-eastern China, respectively (Fig. S1).

Niño 3.4 Index calculated from CMIP6

The Niño 3.4 index from NOAA is the anomaly of SST relative to a 30-year average updated every 5 years over the central-eastern equatorial Pacific (5°N – 5°S , 170°W – 120°W). Guan and Nigam (2008) have indicated that the correlation coefficient between the observed Niño 3.4 index for a century and the synthetic Niño 3.4 index based on the combination of canonical, noncanonical, and biennial modes is 0.95. And according to Nigam and Sengupta (2021), the original Niño 3.4 index correlates with the two-mode index at 0.85, with the three-mode index at 0.87, and with the one that calculated by the total variability of ENSO in temporal and spatial SST analyses at 0.97. Therefore, owing to the high correlation, the Niño index above the Niño 3.4 region has been widely used to present the interannual tropical Pacific SST variability such as ENSO, and also has been seen as the marker to investigate climate change such as precipitation (Nigam and Sengupta 2021).

Thus, in this study, we calculate the Niño index based on monthly mean SST from CMIP6 over the Niño 3.4 region (5°N – 5°S , 170°W – 120°W) during the period 1950–2014. Then we conduct the standardization treatment by the following formulas:

$$X_k = \frac{x_k - \bar{x}}{s}$$

where X_k is the standardized index and \bar{x} and s are the values of average and standard deviation, respectively. Then we define this series as the CMIP6 Niño Index (CNI). In order to find the anomalous SST events (El Niño and La Niña events) and investigate their effects on summertime meteorological conditions and surface ozone concentrations, we define El Niño years as those in which the monthly CNI

value is greater than 1.0 in winter (December/January/February) and greater than 0.5 in all months before next June. In contrast, La Niña years are those in which the monthly CNI value is less than -1.0 in winter (year M) and less than -0.5 in all months until next June (year $M+1$). In the following article, we analyze the values in year $M+1$.

Using this definition of El Niño and La Niña events, the El Niño years are 1954, 1982, 1990, 1998, and 2006, while the La Niña years are 1950, 1964, 1967, 1985, and 1991 (Fig. 2a). The SST in the Niño 3.4 region is anomalously warm during El Niño (Fig. 2b), with a maximum increase of 0.41°C (according to the anomalies during El Niño years). On the contrary, in La Niña events, the SST decreases by 0.45°C on average (Fig. 2c).

Besides, the differences of each meteorological variable averaged over the study period and the El Niño and La Niña years defined by NNI (NOAA Niño 3.4 Index) over 2005–2017 shown in ERA5 (Fig. S2) and CNI (CMIP6 Niño Index) over 1950–2014 shown in CMIP6 (Fig. S3) are similar. The results show that the impacts of simulated and observed ENSO on meteorological conditions are roughly consistent.

Results

Effects of ENSO on summertime surface ozone over central-eastern China

Figure 3 shows the distributions of detrended summertime concentrations of surface ozone over the study period (1950–2014) and the ozone anomalies during El Niño and La Niña events. During the El Niño events, the summertime surface ozone concentrations (30.69 ppb ; Fig. S4) are higher than the 1950–2014 mean (30.25 ppb) by 0.44 ppb averaged over CEC, with the maximum anomalies of 2.88 ppb . By contrast, during the La Niña events, we find negative anomalies of surface ozone over CEC (by 0.91 ppb on average), with the maximum anomalies of 5.52 ppb . The changes of ozone are more significant during the La Niña years (-3.01%) than the El Niño years (1.45%). Meanwhile, the surface ozone data from MPI-ESM-1-2-HAM and EC-Earth3-AerChem show the similar results after doing the same analysis above (Fig. S5).

In order to verify whether the ozone anomalies during ENSO over central-eastern China are robust, we conduct a correlation analysis between the standardized CNI over the Niño 3.4 region and detrended summertime MDA8 ozone concentrations over CEC during 1950–2014 (Fig. 4). On an interannual timescale, the summer ozone pollution over central-eastern China is correlated with the CNI values, with a statistically significant correlation coefficient of 0.29 (P -value = 0.02).

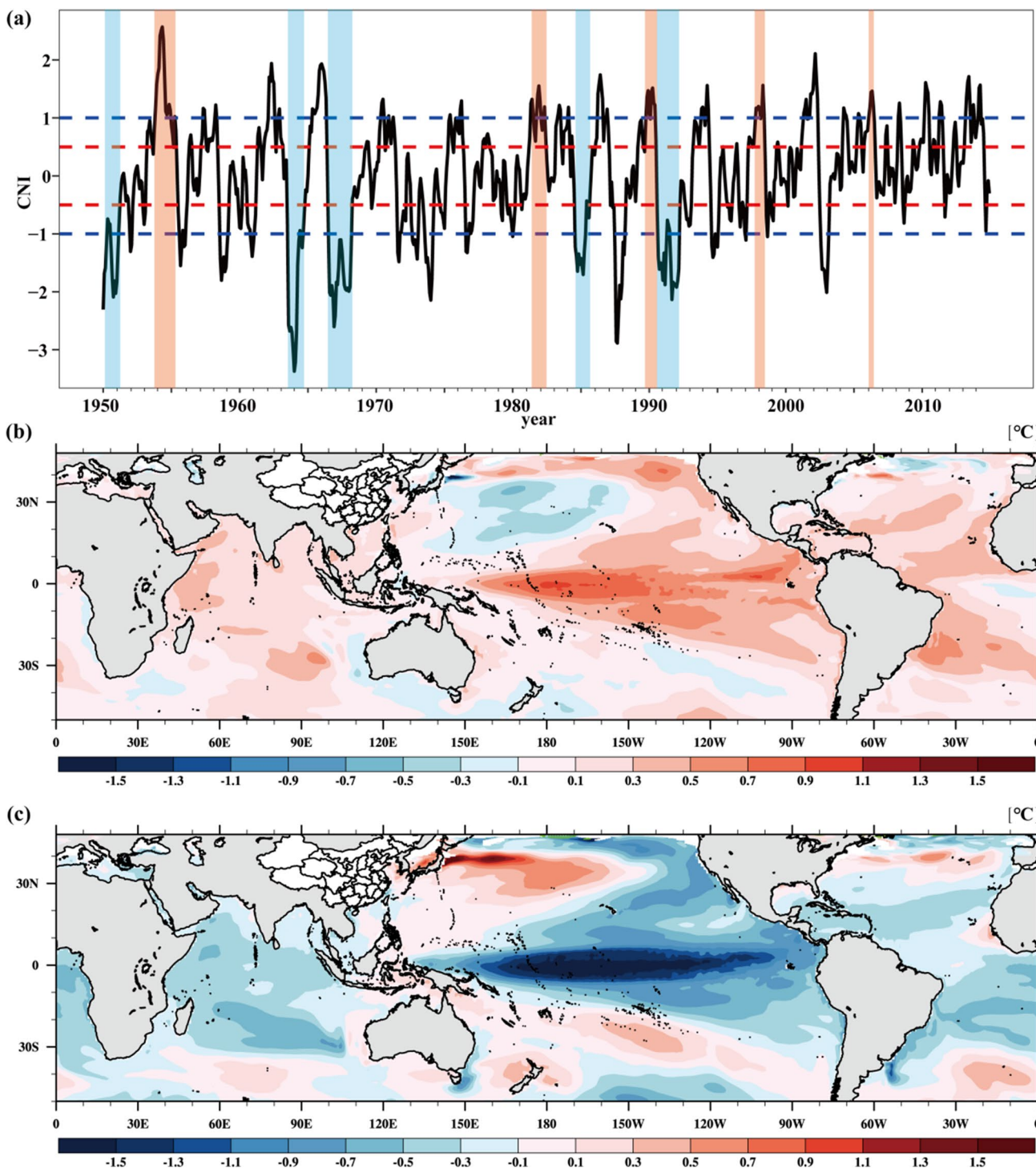


Fig. 2 (a) Monthly time series of CNI during 1950–2014. The red dotted lines mark the values of 0.5 and -0.5 , and the blue dotted lines mark the values of 1 and -1 . The brown shaded bars mark the El

Niño events, while the blue shaded bars mark the La Niña events. The SST anomalies (relative to the 1950–2014 mean) averaged over the El Niño (b) and La Niña (c) events

To validate the simulated ozone-ENSO relationship, we further examine such relationship based on the OMI ozone data and the NOAA Niño 3.4 Index (NNI) over 2005–2017. The NNI is used to define the real El Niño and La Niña

events during 2005–2017, with the actually occurred El Niño years of 2015–2016 and La Niña years of 2011–2012 based on our criteria (Fig. 5a). The opposite distributions of summertime ozone anomalies between El Niño (mainly

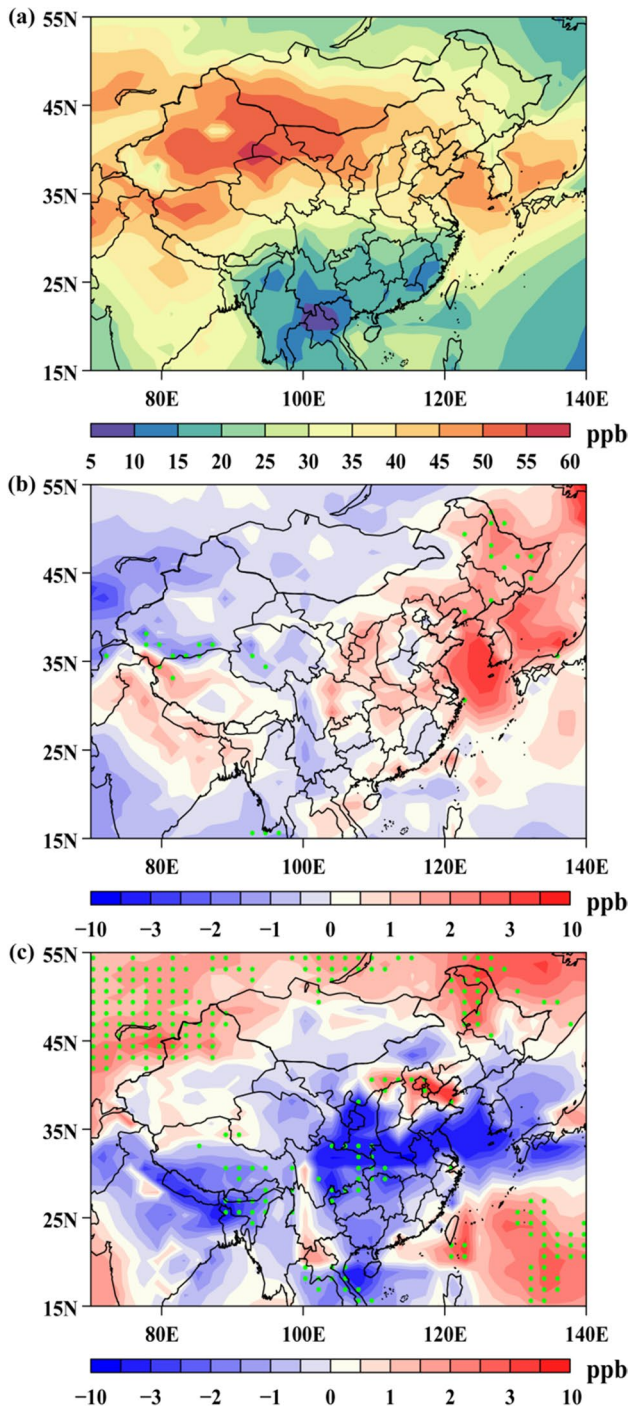


Fig. 3 Spatial distribution of detrended summertime surface ozone concentrations averaged over 1950–2014 (a), as well as the anomalies during El Niño (b) and La Niña (c) years. The green dots indicate the P -value < 0.1

positive anomalies) and La Niña (mainly negative anomalies) events over CEC are shown in the OMI observations (Fig. 5). This result is consistent with that shown in CMIP6, although the CMIP6 ozone anomalies are much smoother and stronger than those shown in the OMI. Such differences

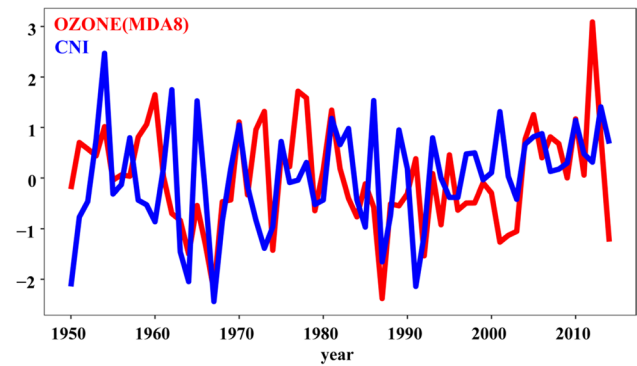


Fig. 4 The red curve represents the time series of detrended summertime MDA8 surface ozone concentrations over central-eastern China, and the blue curve represents the annual time series of CNI over the Niño 3.4 region during 1950–2014 ($R=0.29$, P -value = 0.02)

between CMIP6 and OMI summertime ozone anomalies during ENSO could be partially attributed to their time mismatch and different spatial horizontal resolutions. Moreover, the OMI ozone anomalies are based on single El Niño/La Niña event while the CMIP6 anomalies are the mean values of the El Niño/La Niña years we defined, so the distributions of summertime ozone concentrations are slightly different between the two datasets. According to the NNI, the magnitude of El Niño SST anomaly is much greater than that for La Niña, leading to the larger change of ozone in El Niño years.

Many previous studies have also indicated that the tropospheric ozone will enhance due to the El Niño events. Koumoutsaris et al. (2008) have reported that the tropospheric ozone column was anomalously positive over Europe (4.9 DU at most) during 1997–1998, which was recognized as a strong El Niño year, based on the GEOS-Chem model simulations from 1987 to 2005. According to Voulgarakis et al. (2011), the global tropospheric ozone, especially extratropical tropospheric ozone, has an obvious enhancement in the El Niño event (1998) based on the p-TOMCAT model simulations. Xie et al. (2014) have pointed out that the enhancement of tropospheric ozone during El Niño could also occur in the tropics, with the greatest response over the tropical eastern Pacific. Zeng and Pyle (2005) have found a similar result based on UM/CHEM simulations for 1990–2001.

Causes of ozone anomalies during El Niño and La Niña events

Based on CMIP6 historical simulations, we further analyze the effects of ENSO on summertime meteorological conditions over central-eastern China to understand the causes of ozone anomalies during El Niño and La Niña events. We first discuss the atmospheric circulation indicated by horizontal wind fields and geopotential height over the layers of

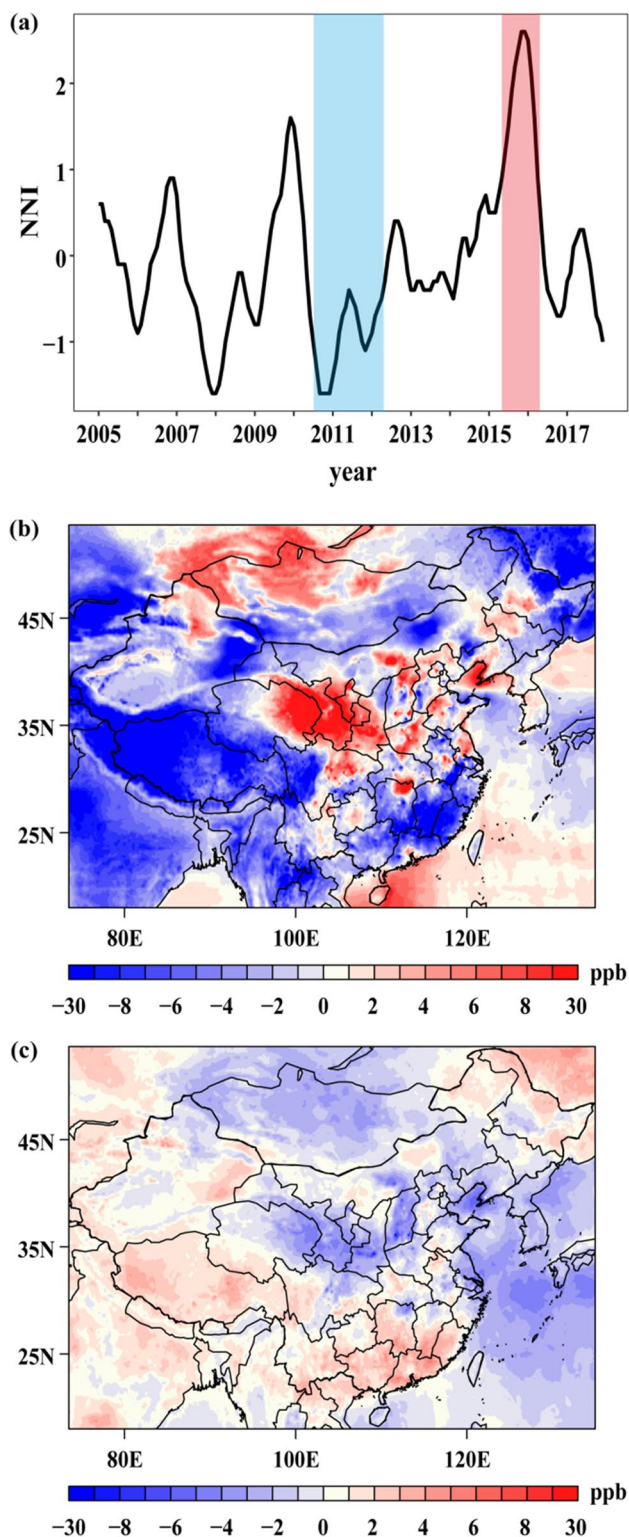


Fig. 5 (a) Monthly time series of NNI during 2005–2017. The red shaded bar marks the El Niño event, and the blue shaded bar marks the La Niña event. The summertime surface ozone anomalies in El Niño (b) and La Niña (c) events calculated based on OMI data

925 hPa, 850 hPa, and 500 hPa. We also analyze the vertical velocity in these three layers as the marker of atmospheric

stability, as well as surface air temperature and precipitation. We separately discuss the northern (31°N–42°N) and southern (20°N–31°N) parts of central-eastern China.

The 1950–2014 average of summertime horizontal wind fields and geopotential height (Fig. 6a) show that, at 925 hPa and 850 hPa, the anticyclone (subtropical high) over the Pacific can be obviously visible. Under the control of anticyclone periphery, there are southerly winds (East Asian Summer Monsoon) in most parts of CEC during summer, with the mean wind speeds of 1.71 m s^{-1} on 850 hPa. While during El Niño and La Niña events, the location, intensity, and pattern of subtropical high over the Pacific are different (Fig. S6), which can influence the transport of warm moist air flow from tropical ocean to central-eastern China. Under the combined action of warm moisture flow and varied atmospheric stability (indicated by the vertical velocity; Fig. 7), the surface air temperature (Fig. 8) and the precipitation distribution (Fig. 9) can be further affected. Thus the specific summertime meteorological conditions caused by El Niño and La Niña events in central-eastern China will dominate the ozone levels and distributions by enhancing/weakening the production and diffusion of ozone.

Specifically, during El Niño events, the atmospheric circulation anomalies show two cyclones (low-pressure system) over the Okhotsk Ocean and Eastern Pacific, as well as an anticyclone (high-pressure system) over the subtropical western Pacific (Fig. 6b), leading to a weaker center intensity but stronger peripheral intensity, and a more eastern-southern location of subtropical high (Fig. S6a). Thus the atmospheric pressure is enhanced over most region of central-eastern China (Fig. 6b), with a maximum increase of 3.73 m for the 850-hPa geopotential height (1452.87 m on average). The more eastern-southern location of subtropical high ridge leads to more warm air full of water vapor to southern part of CEC. Thus the anomalous surface air temperature is significantly positive in the southern part of CEC and North China, while slightly negative over the middle part of CEC (Fig. 8b), affected by the integration of abnormal high air pressure and warm air flow.

In addition, for the summertime precipitation, there is more precipitation in southern part of central-eastern China and less precipitation in northern part (Fig. 9b), with the El Niño averages of 281.71 kg m^{-2} (south) and 91.92 kg m^{-2} (north) versus the climatological averages of 271.34 kg m^{-2} (south) and 96.89 kg m^{-2} (north). The precipitation is 3.82/5.13% higher/lower in the southern/northern region compared to the climatological average. In addition to the moisture over southern part of CEC, it is also attributed to the strengthened (6.45% on average over 850 hPa) vertical ascend movement, while weakened (300% on average over 500 hPa) over the northern region (Fig. 7b, Fig. S7, and Table 1). Feng et al. (2011) have also shown that in the subsequent summer of decaying El Niño events, the precipitation is more in the southern Yangtze River,

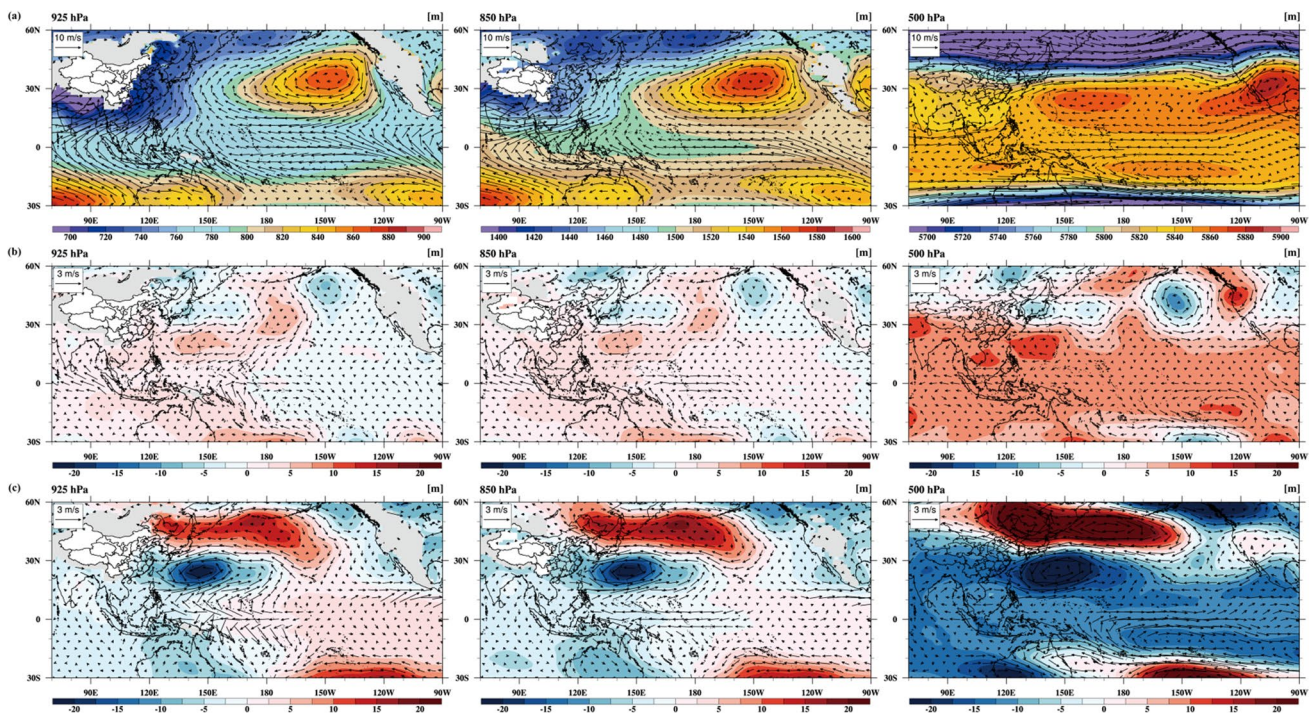


Fig. 6 Spatial distributions of summertime horizontal wind fields and geopotential height at 925 hPa, 850 hPa, and 500 hPa averaged over 1950–2014 (a), as well as the anomalies during El Niño (b) and La

Niña (c) years. The missing values shown in gray areas are not provided by CMIP6 simulations because of the topographic

while a dry signal appears in the north of Yangtze River. Similar conclusions can also be found in the study of Wen et al. (2020). For summer East Pacific El Niño, under the control of anomalous low-pressure system over the north-east of Asia, the rain belt is located in Southeast China, leading to abnormal drought in North China.

Above all, in El Niño events, affected by anomalous high/low-pressure system over the south/north-east of Asia, the southern part of CEC show abnormal warm and humid (cloudy and rainy) meteorological conditions and the northern part become abnormal high temperature and drought. As a result, over the northern part of CEC, the high-temperature and low-humidity circumstance is favorable to improve the photochemical formation efficiency of ozone. Meanwhile, the weakened vertical ascending movement from the lower troposphere to the upper troposphere over here lead to stable atmospheric conditions, which is adverse to the diffusion of ozone and its precursors. While over the southern part of CEC, the overcast and rainy atmospheric condition is not suitable for the photochemical reaction of ozone. Moreover, the strengthened vertical ascend motion will enhance the ozone diffusion. Therefore, the ozone concentrations are lower over most region of southern CEC, while the most part of northern CEC is at higher level of summertime surface ozone.

By contrast, in La Niña events, the situations are exactly opposite. For atmospheric circulation anomalies, the location

of subtropical high over the Pacific is more western-northern (Fig. S6b). The anomalies of geopotential height at 925 hPa, 850 hPa, and 500 hPa show an anticyclone (high-pressure system) over the north-east of Asia, extending to the eastern North Pacific, and a cyclone (low-pressure system) over the subtropical western Pacific. Moreover, similar to the El Niño events, the atmospheric circulation anomalies become stronger as the increasing of height. The averaged geopotential height is 1445.89 m on 850 hPa over central-eastern China, with the maximum decrease of 9.67 m. Such anomalies of atmospheric circulation in La Niña events are at higher degree and more significant than those of El Niño events (Fig. 6c). Thus the warm moisture flow from the Bay of Bengal and across equator bypasses the southern region of CEC along the South China Sea and East China Sea, and enters the northern region of CEC and North China from the Yellow Sea and Bohai Sea.

Meanwhile, the vertical velocity shows an enhanced (125% on average over 850 hPa)/weakened (2.04% on average over 500 hPa) ascending air flow occurring in the north/south part of CEC (Fig. 7c and Table 1), associated with the atmospheric circulation anomalies. Combined with the northward movement of water vapor channel, the anomalous precipitation shows positive/negative values over north/south part of CEC. The summertime precipitation is more/less over northern/southern CEC, with the average precipitation of 112.78 kg m^{-2} (north; 16.40% higher) and

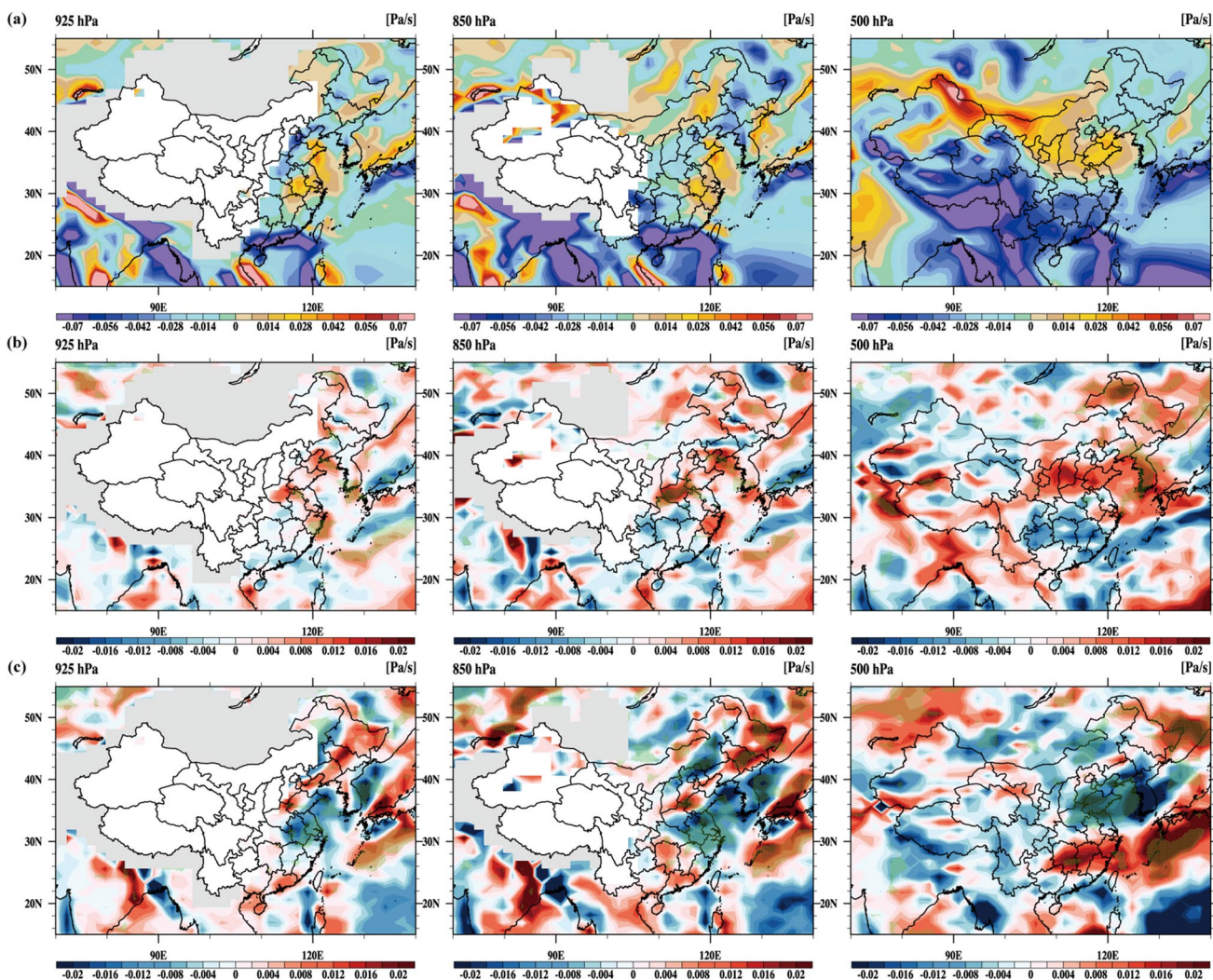


Fig. 7 Spatial distributions of summertime vertical velocity at 925 hPa, 850 hPa, and 500 hPa averaged over 1950–2014 (a), as well as the anomalies in El Niño (b) and La Niña (c) events. The green

dots indicate the *P*-value < 0.1. The missing values shown in gray areas are not provided by CMIP6 simulations because of the topographic

265.15 kg m⁻² (south; 2.28% lower), respectively (Fig. 9c). In addition, even though a negative anomaly of temperature is shown over whole CEC (22.35 °C versus 22.89 °C; 2.36% lower), a positive temperature anomaly is shown in the north-east of China (Fig. 8c).

During the La Niña events, as we discussed above, the atmospheric circulations show an anomalous high/low-pressure system over the north/south-east of Asia. In the north part of CEC, there are enhanced ascending air flows and more precipitation. Such meteorological conditions are beneficial for the diffusion of ozone and its precursors but against to form ozone via photochemical processes. The ozone concentrations are significantly mitigated over northern CEC, with the maximum decrease up to 10 ppb (Fig. 3c). While, in the south of CEC, the weakened vertical ascent is on behalf of more stable atmosphere,

conductive to the accumulation of ozone. Moreover, less precipitation is good for ozone photochemical efficiency. Thus, the decline of ozone in south part caused by lower temperature can be partly offset, even with an enhanced surface ozone occurred over southeast coast, especially the Pearl River Delta and Yangtze River Delta (Fig. 3c). Such North–South difference of ozone anomaly over CEC during ENSO is more obvious in the OMI observations.

Discussion and conclusions

Although there are many studies which have discussed that the El Niño and La Niña events can impact the tropospheric ozone (Zeng and Pyle 2005; Koumoutsaris et al. 2008; Hitchman and Rogal 2010; Lee et al. 2010; Voulgarakis

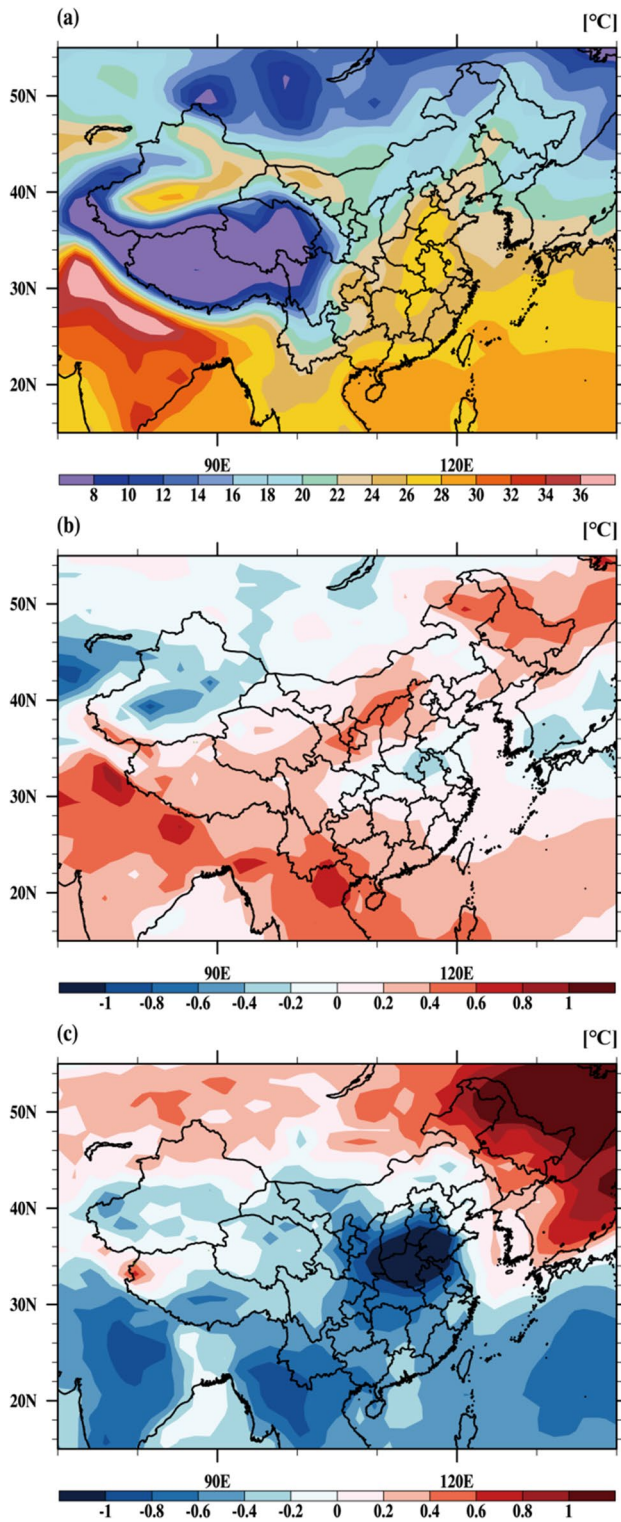


Fig. 8 Spatial distributions of summertime surface air temperature averaged over 1950–2014 (a), as well as the anomalies in El Niño (b) and La Niña (c) events

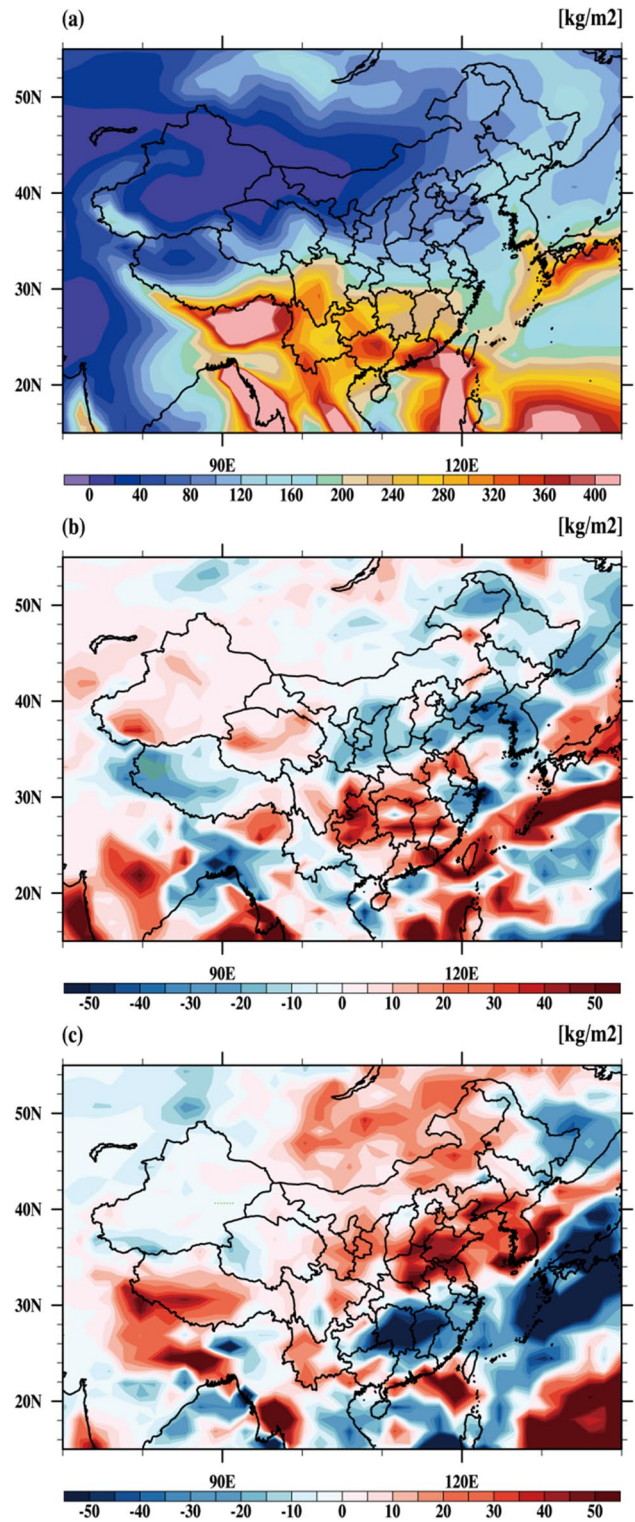


Fig. 9 Spatial distributions of summertime precipitation averaged over 1950–2014 (a), as well as the anomalies in El Niño (b) and La Niña (c) events

Table 1 Statistics of SST, GH (geopotential height), VV (vertical velocity), SAT (surface air temperature), PRE (precipitation), and surface ozone concentrations averaged over 1950–2014 and in the El Niño/La Niña events

Variable	1950–2014				El Niño				La Niña			
	Max	Min	Ave		Max	Min	Ave		Max	Min	Ave	
SST (°C)	28.59	26.72	27.81		28.84	27.08	28.13 (1.15%)		28.16	26.23	27.36 (-1.62%)	
925-hPa GH (m)	790.71	699.27	720.43		736.60	700.07	721.50 (0.15%)		788.48	695.46	716.30 (-0.57%)	
850-hPa GH (m)	1539.35	1436.29	1451.50		1499.69	1437.97	1452.87 (0.09%)		1496.59	1430.80	1445.89 (-0.39%)	
500-hPa GH (m)	5841.38	5716.81	5804.23		5851.54	5717.54	5810.27 (0.10%)		5824.77	5730.69	5793.73 (-0.18%)	
925-hPa VV (Pa/s) (N; S)	0.044; 0.030	-0.076; -0.124	-0.008; -0.021		0.045; 0.030	-0.080; -0.130	-0.006 (-25.00%); -0.022 (4.76%)		0.032; 0.026	-0.070; -0.145	-0.012 (50.00%); -0.022 (4.76%)	
850-hPa VV (Pa/s) (N; S)	0.052; 0.046	-0.047; -0.144	-0.004; -0.031		0.047; 0.036	-0.049; -0.156	-0.002 (-50.00%); -0.033 (6.45%)		0.031; 0.038	-0.052; -0.169	-0.009 (125.00%); -0.032 (3.23%)	
500-hPa VV (Pa/s) (N; S)	0.055; -0.012	-0.081; -0.115	-0.004; -0.049		0.055; -0.004	-0.074; -0.130	0.008 (-300.00%); -0.051 (4.08%)		0.061; -0.010	-0.084; -0.147	-0.002 (-50.00%); -0.048 (-2.04%)	
SAT (°C)	29.75	6.90	22.89		30.18	7.21	23.09 (0.87%)		29.14	6.65	22.35 (-2.36%)	
PRE (kg/m ²) (N; S)	246.70; 594.57	6.81; 160.79	96.89; 271.34		247.41; 658.76	8.13; 95.09	91.92 (-5.13%); 281.71 (3.82%)		253.35; 704.69	8.56; 140.52	112.78 (16.40%); 265.15 (-2.28%)	
Surface ozone concentration (ppb)	52.54	6.31	30.25		52.55	5.60	30.69 (1.45%)		51.85	7.80	29.34 (-3.01%)	

The normalized anomalies during El Niño/La Niña events are also shown in brackets. The SST is calculated for the Niño 3.4 region; the GH, SAT, and summertime surface ozone for central-eastern China; and the VV and PRE for the northern and southern parts of central-eastern China, respectively

et al. 2010; Ziemke et al. 2010; Oman et al. 2011; Voulgarakis et al. 2011; Xie et al. 2014; Zhang et al. 2015; Ziemke et al. 2015; Yang et al. 2022) by influencing the changes of troposphere-stratosphere exchange, because of the meteorological variabilities (temperature, winds, and humidity) and dynamic changes, few studies focus on the effect of ENSO on surface ozone, an increasingly severe air pollution all over the world. In addition, except for several researches that pay attention to the linkage between El Niño, La Niña, and surface ozone levels in tropical and northern midlatitude (Shen and Mickley 2017; Xu et al. 2017), there are few researches to discuss the long-term situations, especially in China, due to the lack of historical ozone observations. Li et al. (2022) have used the GEOS-Chem model to investigate the influence of ENSO on summertime near-surface ozone in China by choosing the two strong El Niño events. The results have shown that the El Niño events increase the near-surface ozone concentrations over northeastern and southern China by 6 ppb and 3 ppb, respectively, due to the hot and dry weather as well as weakened wind. And over the United States, according to Shen and Mickley (2017), the El Niño events during 1980–2016 could lead to less humid clean air flows to the Atlantic states, which would make less precipitation and stronger solar radiation in summer. Meanwhile, the transportation and diffusion of pollutants would be improved in the south central states. As a result, the ozone concentrations increased 1–2 ppb in the Atlantic states, but decreased 0.5–2 ppb in the south central states.

In our study, we use the modeled historical surface ozone from CMIP6 and its matched meteorological simulations. Our study explores the effects of ENSO on summertime surface ozone in central-eastern China during the period of 1950–2014. Our results show that the more eastern-southern location of subtropical high during the El Niño events will regulate the atmospheric circulation and meteorological conditions of CEC. As a result, under the interaction of meteorological factors, atmospheric stability as well as synoptic circulations, the diffusion and formation of ozone could be influenced, leading to an enhanced the summertime ozone concentrations up to 52.55 ppb over northern CEC (with the maximum difference of 2.88 ppb), while a lower level of ozone in some part of southern CEC. On the contrary, during the La Niña events, affected by the western-northern location of subtropical high, the water vapor transport channel bypasses the southern CEC and moves northward. Therefore, the detrended summertime surface ozone concentrations have been decreased to 29.34 ppb on average (with the maximum difference of 5.52 ppb), and the weakened degree of ozone in south part is slighter than north part. In addition, as the decrease of SST over the Niño 3.4 region in La Niña events (0.45 °C) is greater than the increase of that in El Niño events (0.32 °C), a greater change degree of surface ozone could be found in La Niña (−3.01%) than El Niño (1.45%). The similar

results can also be visible in the surface ozone observed by satellite (OMI) and the North–South difference of ozone anomaly over CEC during ENSO is more obvious in the OMI observations. Our study also shows that, in interannual timescale, the summertime surface ozone of CEC is significantly correlated with the CMIP6 Niño Index, with $R=0.29$ and $P\text{-value}=0.02$.

Our study explores the effect of climate system on surface ozone in a long timescale over China. The results could make better estimation and attribution of future surface ozone pollution in China. However, the limitations of our study are embodied in the lack of ground ozone observations to verify the historical simulated results. In addition, the way to exclude the effect of anthropogenic emission is oversimplified. The increasing trend of surface ozone is not only emission-related but also slightly related to meteorology. Therefore, the effect of climate variability on surface ozone may be underestimate in our research.

Supplementary Information The online version contains supplementary material available at <https://doi.org/10.1007/s11356-022-22543-6>.

Acknowledgements We acknowledge the free use of CMIP6 model simulations.

Author contribution Yuexuanzi Wang: methodology, investigation, data curation, writing—original draft. Yingying Yan: conceptualization, methodology, writing—review and editing. Jintai Lin: supervision, review and editing. Shaofei Kong: supervision, review and editing. Aili Song: data curation. Jing Ma: data curation.

Funding This study was supported by the National Natural Science Foundation of China (41905112; 41830965), the China Postdoctoral Science Foundation funded project (258572), the Key Program of Ministry of Science and Technology of the People's Republic of China (2017YFC0212602), and the Innovation Training Program for College Students (202110491065).

Data availability The modeled hourly surface ozone is from CMIP6 (<https://cera-www.dkrz.de/WDCC/ui/cersearch/cmip6?input=CMIP6.CMIP.MOHC.UKESM1-0-LL.historical/>). Ozone satellite retrieval data of OMI is from <https://www.cfa.harvard.edu/atmosphere/>.

Declarations

Ethics approval Not applicable.

Consent to participate Not applicable.

Consent for publication Not applicable.

Competing interests The authors declare no competing interests.

References

Bjerknes J (1972) Large-scale atmospheric response to the 1964–65 Pacific equatorial warming. *J Phys Oceanogr* 2:212–217. <https://doi.org/10.1029/JPO70212>

- [doi.org/10.1175/1520-0485\(1972\)002%3c0212:LSARTT%3e2.0.CO;2](https://doi.org/10.1175/1520-0485(1972)002%3c0212:LSARTT%3e2.0.CO;2)
- Bracegirdle TJ, Krinner G, Tonelli M, Haumann FA, Naughten KA, Rackow T, Roach LA, Wainer I (2020) Twenty first century changes in Antarctic and Southern Ocean surface climate in CMIP6. *Atmos Sci Lett* 21. <https://doi.org/10.1002/asl.984>
- Butchart N, Anstey JA, Kawatani Y, Osprey SM, Richter JH, Wu TW (2020) QBO changes in CMIP6 climate projections. *Geophys Res Lett* 47:e984. <https://doi.org/10.1029/2019gl086903>
- Chandra S, Ziemke JR, Min W, Read WG (1998) Effects of 1997–1998 El Niño on tropospheric ozone and water vapor. *Geophys Res Lett* 25:3867–3870. <https://doi.org/10.1029/98GL02695>
- Chang CP, Zhang YS, Li T (2000) Interannual and interdecadal variations of the East Asian summer monsoon and tropical Pacific SSTs. Part I: Roles of the Subtropical Ridge. *Journal of Climate* 13:4310–4325. [https://doi.org/10.1175/1520-0442\(2000\)013%3c4310:IAIVOT%3e2.0.CO;2](https://doi.org/10.1175/1520-0442(2000)013%3c4310:IAIVOT%3e2.0.CO;2)
- Chen X, Zhong BQ, Huang FX, Wang XM, Sarkar S, Jia SG, Deng XJ, Chen DH, Shao M (2020) The role of natural factors in constraining long-term tropospheric ozone trends over Southern China. *Atmos Environ* 220:11. <https://doi.org/10.1016/j.atmosenv.2019.117060>
- David LM, Nair PR (2011) Diurnal and seasonal variability of surface ozone and NO_x at a tropical coastal site: association with mesoscale and synoptic meteorological conditions. *Journal of Geophysical Research-Atmospheres* 116. <https://doi.org/10.1029/2010jd015076>
- Davies TD, Kelly PM, Low PS, Pierce CE (1992) Surface ozone concentrations in Europe: links with the regional-scale atmospheric circulation. *Journal of Geophysical Research: Atmospheres* 97:9819–9832. <https://doi.org/10.1029/92JD00419>
- Ding AJ, Wang T, Zhao M, Wang TJ, Li ZK (2004) Simulation of sea-land breezes and a discussion of their implications on the transport of air pollution during a multi-day ozone episode in the Pearl River Delta of China. *Atmos Environ* 38:6737–6750. <https://doi.org/10.1016/j.atmosenv.2004.09.0>
- Duan JC, Tan JH, Yang L (2008) Concentration, sources and ozone formation potential of volatile organic compounds (VOCs) during ozone episode in Beijing. *Atmos Res* 88:25–35. <https://doi.org/10.1016/j.atmosres.2007.09.004>
- Emberson, L.: Effects of ozone on agriculture, forests and grasslands, *Philosophical Transactions of the Royal Society A-Mathematical Physical and Engineering Sciences*, 378, <https://doi.org/10.1098/rsta.2019.0327>, 2020.
- Eyring V, Bony S, Meehl GA, Senior CA, Stevens B, Stouffer RJ, Taylor KE (2016) Overview of the Coupled Model Intercomparison Project Phase 6 (CMIP6) experimental design and organization. *Geoscientific Model Development* 9:1937–1958. <https://doi.org/10.5194/gmd-9-1937-2016>
- Feng J, Chen W, Tam CY, Zhou W (2011) Different impacts of El Niño and El Niño Modoki on China rainfall in the decaying phases. *Int J Climatol* 31:2091–2101. <https://doi.org/10.1002/joc.2217>
- Griffiths PT, Murray LT, Zeng G, Archibald AT, Emmons LK, Galbally I, Hassler B, Horowitz LW, Keeble J, Liu J, Moeini O, Naik V, O'Connor FM, Shin YM, Tarasick D, Tilmes S, Turnock ST, Wild O, Young PJ, Zanis P (2021) Tropospheric ozone in CMIP6 simulations. *Atmos Chem Phys Discuss*. <https://doi.org/10.5194/acp-2019-1216>
- Guan B, Nigam S (2008) Pacific sea surface temperatures in the twentieth century: an evolution-centric analysis of variability and trend. *J Clim* 21:2790–2809. <https://doi.org/10.1175/2007JCLI2076.1>
- Han H, Liu JE, Shu L, Wang TJ, Yuan HL (2020) Local and synoptic meteorological influences on daily variability in summertime surface ozone in eastern China. *Atmos Chem Phys* 20:203–222. <https://doi.org/10.5194/acp-20-203-2020>
- He JJ, Gong SL, Yu Y, Yu LJ, Wu L, Mao HJ, Song CB, Zhao SP, Liu HL, Li XY, Li RP (2017) Air pollution characteristics and their relation to meteorological conditions during 2014–2015 in major Chinese cities. *Environ Pollut* 223:484–496. <https://doi.org/10.1016/j.envpol.2017.01.050>
- Hitchman MH, Rogal MJ (2010) ENSO influences on Southern Hemisphere column ozone during the winter to spring transition. *Journal of Geophysical Research-Atmospheres* 115. <https://doi.org/10.1029/2009jd012844>
- Hou XW, Zhu B, Fei DD, Wang DD (2015) The impacts of summer monsoons on the ozone budget of the atmospheric boundary layer of the Asia-Pacific region. *Sci Total Environ* 502:641–649. <https://doi.org/10.1016/j.scitotenv.2014.09.075>
- Jacob DJ, Winner DA (2009) Effect of climate change on air quality. *Atmos Environ* 43:51–63. <https://doi.org/10.1016/j.atmosenv.2008.09.051>
- Jiang Z, Li J (2022) Impact of eastern and central Pacific El Niño on lower tropospheric ozone in China. *Atmos Chem Phys* 22:7273–7285
- Koumoutsaris S, Bey I, Generoso S, Thouret V (2008) Influence of El Niño–Southern Oscillation on the interannual variability of tropospheric ozone in the northern midlatitudes. *Journal of Geophysical Research: Atmospheres* 113. <https://doi.org/10.1029/2007JD009753>
- Lee S, Shelow DM, Thompson AM, Miller SK (2010) QBO and ENSO variability in temperature and ozone from SHADOZ, 1998–2005. *Journal of Geophysical Research-Atmospheres* 115. <https://doi.org/10.1029/2009jd013320>
- Li K, Chen LH, Ying F, White SJ, Jang C, Wu XC, Gao X, Hong SM, Shen JD, Azzi M, Cen KF (2017) Meteorological and chemical impacts on ozone formation: a case study in Hangzhou, China. *Atmospheric Research* 196:40–52. <https://doi.org/10.1016/j.atmosres.2017.06.003>
- Li K, Jacob DJ, Liao H, Shen L, Zhang Q, Bates KH (2019) Anthropogenic drivers of 2013–2017 trends in summer surface ozone in China. *Proc Natl Acad Sci USA* 116:422–427. <https://doi.org/10.1073/pnas.1812168116>
- Li K, Jacob DJ, Shen L, Lu X, De Smedt I, Liao H (2020) Increases in surface ozone pollution in China from 2013 to 2019: anthropogenic and meteorological influences. *Atmos Chem Phys* 20:11423–11433. <https://doi.org/10.5194/acp-20-11423-2020>
- Li M, Yang Y, Wang P, Ji D, Liao H (2022) Impacts of strong El Niño on summertime near-surface ozone over China. *Atmos Ocean Sci Lett* 15:100193
- Liao ZH, Gao M, Sun JR, Fan SJ (2017) The impact of synoptic circulation on air quality and pollution-related human health in the Yangtze River Delta region. *Sci Total Environ* 607:838–846. <https://doi.org/10.1016/j.scitotenv.2017.07.031>
- Lin M, Horowitz LW, Payton R, Fiore AM, Tonnesen G (2017) US surface ozone trends and extremes from 1980 to 2014: quantifying the roles of rising Asian emissions, domestic controls, wildfires, and climate. *Atmos Chem Phys* 17:2943–2970. <https://doi.org/10.5194/acp-17-2943-2017>
- Lippmann M (1989) Health effects of ozone: a critical review. *JAPCA* 39:672–695. <https://doi.org/10.1080/08940630.1989.10466554>
- Liu H, Liu S, Xue BR, Lv ZF, Meng ZH, Yang XF, Xue T, Yu Q, He KB (2018) Ground-level ozone pollution and its health impacts in China. *Atmos Environ* 173:223–230. <https://doi.org/10.1016/j.atmosenv.2017.11.014>
- Lu X, Zhang L, Chen YF, Zhou M, Zheng B, Li K, Liu YM, Lin JT, Fu TM, Zhang Q (2019) Exploring 2016–2017 surface ozone pollution over China: source contributions and meteorological influences. *Atmos Chem Phys* 19:8339–8361. <https://doi.org/10.5194/acp-19-8339-2019>
- Ma ZQ, Zhang XL, Xu J, Zhao XJ, Meng W (2011) Characteristics of ozone vertical profile observed in the boundary layer around

- Beijing in autumn. *J Environ Sci* 23:1316–1324. [https://doi.org/10.1016/s1001-0742\(10\)60557-8](https://doi.org/10.1016/s1001-0742(10)60557-8)
- Ma JZ, Xu XB, Zhao CS, Yan P (2012) A review of atmospheric chemistry research in China: photochemical smog, haze pollution, and gas-aerosol interactions. *Adv Atmos Sci* 29:1006–1026. <https://doi.org/10.1007/s00376-012-1188-7>
- Ma ZQ, Xu J, Quan WJ, Zhang ZY, Lin WL, Xu XB (2016) Significant increase of surface ozone at a rural site, north of eastern China. *Atmos Chem Phys* 16:3969–3977. <https://doi.org/10.5194/acp-16-3969-2016>
- Monks PS, Archibald AT, Colette A, Cooper O, Coyle M, Derwent R, Fowler D, Granier C, Law KS, Mills GE, Stevenson DS, Tarasova O, Thouret V, von Schneidemesser E, Sommariva R, Wild O, Williams ML (2015) Tropospheric ozone and its precursors from the urban to the global scale from air quality to short-lived climate forcer. *Atmos Chem Phys* 15:8889–8973. <https://doi.org/10.5194/acp-15-8889-2015>
- Narsey SY, Brown JR, Colman RA, Delage F, Power SB, Moise AF, Zhang H (2020) Climate change projections for the Australian monsoon from CMIP6 models. *Geophys Res Lett* 47. <https://doi.org/10.1029/2019gl086816>
- Nigam S, Sengupta A (2021) The full extent of El Niño's precipitation influence on the United States and the Americas: the suboptimality of the Niño 3.4 SST index. *Geophys Res Lett* 48. <https://doi.org/10.1029/2020gl091447>
- Nuvolone D, Petri D, Voller F (2018) The effects of ozone on human health. *Environ Sci Pollut Res* 25:8074–8088. <https://doi.org/10.1007/s11356-017-9239-3>
- Oman LD, Ziemke JR, Douglass AR, Waugh DW, Lang C, Rodriguez JM, Nielsen JE (2011) The response of tropical tropospheric ozone to ENSO. *Geophys Res Lett* 38. <https://doi.org/10.1029/2011gl047865>
- O'Neill BC, Tebaldi C, van Vuuren DP, Eyring V, Friedlingstein P, Hurtt G, Knutti R, Krieger E, Lamarque JF, Lowe J, Meehl GA, Moss R, Riahi K, Sanderson BM (2016) The Scenario Model Intercomparison Project (ScenarioMIP) for CMIP6. *Geoscientific Model Development* 9:3461–3482. <https://doi.org/10.5194/gmd-9-3461-2016>
- Otero N, Sillmann J, Schnell JL, Rust HW, Butler T (2016) Synoptic and meteorological drivers of extreme ozone concentrations over Europe. *Environ Res Lett* 11. <https://doi.org/10.1088/1748-9326/11/2/024005>
- Philander SGH (1985) El Niño and La Niña. *Journal of Atmospheric Sciences* 42:2652–2662. [https://doi.org/10.1175/1520-0469\(1985\)042%3c2652:ENALN%3e2.0.CO;2](https://doi.org/10.1175/1520-0469(1985)042%3c2652:ENALN%3e2.0.CO;2)
- Quan XW, Diaz HF, Hoerling MP (2004) Change in the tropical Hadley cell since 1950, in: *The Hadley circulation: present, past and future*, Springer, 85–120. https://doi.org/10.1007/978-1-4020-2944-8_3
- Shen L, Mickley LJ (2017) Effects of El Niño on summertime ozone air quality in the eastern United States. *Geophys Res Lett* 44:12543–12550. <https://doi.org/10.1002/2017gl076150>
- Shen L, Jacob DJ, Liu X, Huang GY, Li K, Liao H, Wang T (2019) An evaluation of the ability of the Ozone Monitoring Instrument (OMI) to observe boundary layer ozone pollution across China: application to 2005–2017 ozone trends. *Atmos Chem Phys* 19:6551–6560. <https://doi.org/10.5194/acp-19-6551-2019>
- Shu L, Xie M, Wang TJ, Gao D, Chen PL, Han Y, Li S, Zhuang BL, Li MM (2016) Integrated studies of a regional ozone pollution synthetically affected by subtropical high and typhoon system in the Yangtze River Delta region, China. *Atmos Chem Phys* 16:15801–15819. <https://doi.org/10.5194/acp-16-15801-2016>
- Sillman S, Logan JA, Wofsy SC (1990) The sensitivity of ozone to nitrogen-oxides and hydrocarbons in regional ozone episodes. *Journal of Geophysical Research Atmospheres* 95:1837–1851. <https://doi.org/10.1029/JD095iD02p01837>
- Sudo K, Takahashi M (2001) Simulation of tropospheric ozone changes during 1997–1998 El Niño: meteorological impact on tropospheric photochemistry. *Geophys Res Lett* 28:4091–4094. <https://doi.org/10.1029/2001GL013335>
- Sun L, Xue LK, Wang YH, Li LL, Lin JT, Ni RJ, Yan YY, Chen LL, Li J, Zhang QZ, Wang WX (2019) Impacts of meteorology and emissions on summertime surface ozone increases over central eastern China between 2003 and 2015. *Atmos Chem Phys* 19:1455–1469. <https://doi.org/10.5194/acp-19-1455-2019>
- Voulgarakis A, Savage NH, Wild O, Braesicke P, Young PJ, Carver GD, Pyle JA (2010) Interannual variability of tropospheric composition: the influence of changes in emissions, meteorology and clouds. *Atmos Chem Phys* 10:2491–2506. <https://doi.org/10.5194/acp-10-2491-2010>
- Voulgarakis A, Hadjinicolaou P, Pyle JA (2011) Increases in global tropospheric ozone following an El Niño event: examining stratospheric ozone variability as a potential driver. *Atmos Sci Lett* 12:228–232. <https://doi.org/10.1002/asl.318>
- Wang T, Nie W, Gao J, Xue LK, Gao XM, Wang XF, Qiu J, Poon CN, Meinardi S, Blake D, Wang SL, Ding AJ, Chai FH, Zhang QZ, Wang WX (2010) Air quality during the 2008 Beijing Olympics: secondary pollutants and regional impact. *Atmos Chem Phys* 10:7603–7615. <https://doi.org/10.5194/acp-10-7603-2010>
- Wang T, Xue LK, Brimblecombe P, Lam YF, Li L, Zhang L (2017) Ozone pollution in China: a review of concentrations, meteorological influences, chemical precursors, and effects. *Sci Total Environ* 575:1582–1596. <https://doi.org/10.1016/j.scitotenv.2016.10.081>
- Wang Y, Yan Y, Duan K, Kong S, Lin J, Zheng H, Song A, Zhang Z (2021) Effect of springtime thermal forcing over Tibetan Plateau on summertime ozone in Central China during the period 1950–2019. *Atmos Res* 261. <https://doi.org/10.1016/j.atmosres.2021.105735>
- Wen N, Li L, Luo JJ (2020) Direct impacts of different types of El Niño in developing summer on East Asian precipitation. *Clim Dyn* 55:1087–1104. <https://doi.org/10.1007/s00382-020-05315-1>
- Wennberg PO, Dabdub D (2008) Rethinking ozone production. *SCIENCE-NEW YORK THEN WASHINGTON* 319:1624. <https://doi.org/10.1126/science.1155747>
- Xie F, Li JP, Tian WS, Zhang JK, Shu JC (2014) The impacts of two types of El Niño on global ozone variations in the last three decades. *Adv Atmos Sci* 31:1113–1126. <https://doi.org/10.1007/s00376-013-3166-0>
- Xu L, Yu JY, Schnell JL, Prather MJ (2017) The seasonality and geographic dependence of ENSO impacts on US surface ozone variability. *Geophys Res Lett* 44:3420–3428. <https://doi.org/10.1002/2017gl073044>
- Yan YY, Lin JT, Chen J, Hu L (2016) Improved simulation of tropospheric ozone by a global-multi-regional two-way coupling model system. *Atmos Chem Phys* 16:2381–2400. <https://doi.org/10.5194/acp-16-2381-2016>
- Yan Y, Lin J, He C (2018) Ozone trends over the United States at different times of day. *Atmos Chem Phys* 18:1185–1202. <https://doi.org/10.5194/acp-18-1185-2018>
- Yan Y, Lin J, Pozzer A, Kong S, Lelieveld J (2019) Trend reversal from high-to-low and from rural-to-urban ozone concentrations over Europe. *Atmos Environ* 213:25–36. <https://doi.org/10.1016/j.atmosenv.2019.05.067>
- Yan YY, Zheng H, Kong SF, Lin JT, Yao LQ, Wu FQ, Cheng Y, Niu ZZ, Zheng SR, Zeng X, Yan Q, Wu J, Zheng MM, Liu MY, Ni RJ, Chen LL, Chen N, Xu K, Liu DT, Zhao DL, Zhao TL, Qi SH (2021) On the local anthropogenic source diversities and trans-boundary transport for urban agglomeration ozone mitigation. *Atmos Environ* 245:11. <https://doi.org/10.1016/j.atmosenv.2020.118005>
- Yang Y, Liao H, Li J (2014) Impacts of the East Asian summer monsoon on interannual variations of summertime surface-layer ozone concentrations over China. *Atmos Chem Phys* 14:6867–6879
- Yang Y, Li M, Wang H, Li H, Wang P, Li K, Gao M, Liao H (2022) ENSO modulation of summertime tropospheric ozone over China. *Environ Res Lett* 17:034020

- Zeng G, Pyle JA (2005) Influence of El Niño Southern Oscillation on stratosphere/troposphere exchange and the global tropospheric ozone budget. *Geophys Res Lett* 32. <https://doi.org/10.1029/2004GL021353>
- Zhai PM, Yu R, Guo YJ, Li QX, Ren XJ, Wang YQ, Xu WH, Liu YJ, Ding YH (2016) The Strong El Niño of 2015/16 and its dominant impacts on global and China's climate. *Journal of Meteorological Research* 30:283–297. <https://doi.org/10.1007/s13351-016-6101-3>
- Zhang JP, Zhu T, Zhang QH, Li CC, Shu HL, Ying Y, Dai ZP, Wang X, Liu XY, Liang AM, Shen HX, Yi BQ (2012) The impact of circulation patterns on regional transport pathways and air quality over Beijing and its surroundings. *Atmos Chem Phys* 12:5031–5053. <https://doi.org/10.5194/acp-12-5031-2012>
- Zhang JK, Tian WS, Wang ZW, Xie F, Wang FY (2015) The influence of ENSO on northern midlatitude ozone during the winter to spring transition. *J Clim* 28:4774–4793. <https://doi.org/10.1175/jcli-d-14-00615.1>
- Zhou DR, Ding AJ, Mao HT, Fu CB, Wang T, Chan LY, Ding K, Zhang Y, Liu J, Lu A, Hao N (2013) Impacts of the East Asian monsoon on lower tropospheric ozone over coastal South China. *Environ Res Lett* 8:7. <https://doi.org/10.1088/1748-9326/8/4/044011>
- Ziemke JR, Chandra S, Oman LD, Bhartia PK (2010) A new ENSO index derived from satellite measurements of column ozone. *Atmos Chem Phys* 10:3711–3721. <https://doi.org/10.5194/acp-10-3711-2010>
- Ziemke JR, Douglass AR, Oman LD, Strahan SE, Duncan BN (2015) Tropospheric ozone variability in the tropics from ENSO to MJO and shorter timescales. *Atmos Chem Phys* 15:8037–8049. <https://doi.org/10.5194/acp-15-8037-2015>

Publisher's note Springer Nature remains neutral with regard to jurisdictional claims in published maps and institutional affiliations.

Springer Nature or its licensor holds exclusive rights to this article under a publishing agreement with the author(s) or other rightsholder(s); author self-archiving of the accepted manuscript version of this article is solely governed by the terms of such publishing agreement and applicable law.